

SceneScape: Text-Driven Consistent Scene Generation

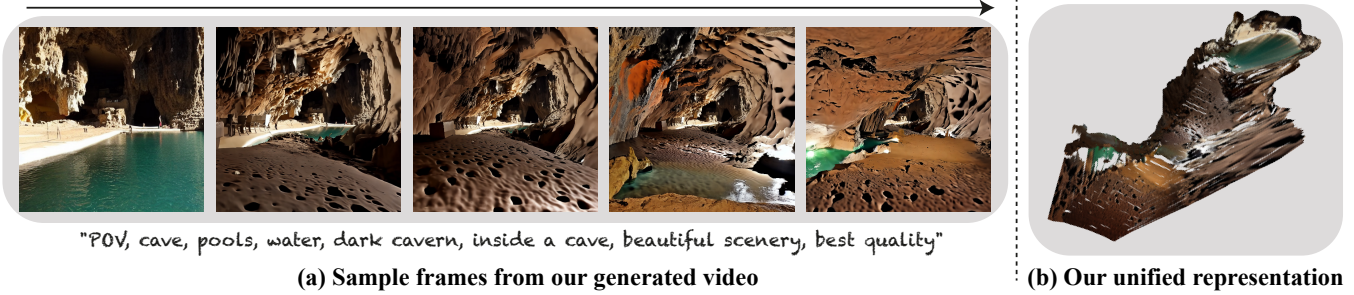
Rafail Fridman¹Amit Abecasis¹Yoni Kasten²Tali Dekel¹¹Weizmann Institute of Science²NVIDIA Research

Figure 1: Text-driven perpetual view generation. (a) Given an input text prompt that describes a scene, our method generates a long-term video that depicts a walkthrough of this scene following a given camera trajectory. We ensure a 3D-consistent scene generation through a unified 3D representation of the scene (b), which is constructed along with the video. For visualization purposes, we remove the top part of the presented mesh.

ABSTRACT

We propose a method for *text-driven perpetual view generation* – synthesizing long videos of arbitrary scenes solely from an input text describing the scene and camera poses. We introduce a novel framework that generates such videos in an online fashion by combining the generative power of a pre-trained text-to-image model with the geometric priors learned by a pre-trained monocular depth prediction model. To achieve 3D consistency, i.e., generating videos that depict geometrically-plausible scenes, we deploy an online test-time training to encourage the predicted depth map of the current frame to be geometrically consistent with the synthesized scene; the depth maps are used to construct a *unified* mesh representation of the scene, which is updated throughout the generation and is used for rendering. In contrast to previous works, which are applicable only for limited domains (e.g., landscapes), our framework generates diverse scenes, such as walkthroughs in spaceships, caves, or ice castles. ¹ Project page: <https://scenescape.github.io/>

1 INTRODUCTION

By observing only a single photo of a scene, we can imagine what it would be like to explore it, move around, or turn our head and look around – we can envision the 3D world captured in the image and expand it in our mind. However, achieving this capability computationally – generating a long-term video that depicts a plausible visual world from an input image – poses several key challenges. One of the main challenges is ensuring that the synthesized content is consistent with a feasible 3D world. For example, it must correctly depict parallax effects and occlusion relations of different objects in the scene. Additionally, to synthesize new content, a strong prior about the visual world and how it would appear beyond the current field of view is necessary. Finally, the generated content should appear smooth and consistent over time.

Previous methods have tackled the task of perpetual view generation for specific domains, for example, synthesizing landscape fly-throughs (e.g., [5, 21, 22]), or bedrooms walkthroughs (e.g., [35, 40]). These methods involve large-scale training on videos or images from the target domain, which limits their use. In this work, inspired by the transformative progress in text-to-image generation, we take a different route and propose a new framework for *text-driven perpetual view generation* – synthesizing long-range videos of scenes solely from free-vocabulary text describing the scene and camera poses. Our method does not require any training data but rather generates the scene in a zero-shot manner by harnessing the generative prior learned by a pre-trained text-to-image diffusion model and the geometric priors learned by a pre-trained depth prediction model.

More specifically, given an input text prompt and a camera trajectory, our framework generates the scene in an online fashion, one frame at a time. The text-to-image diffusion model is used to synthesize new content revealed as the camera moves, whereas the depth prediction model allows us to estimate the geometry of the newly generated content. To ensure that the generated scene adheres to a feasible 3D geometry, our framework estimates a unified mesh representation of the scene that is constructed progressively as the camera moves in the scene. Since monocular depth predictions tend to be flickery and inconsistent across different frames, we finetune the depth prediction model at test time to match the projected depth from our mesh representation for the known, previously synthesized content. This results in a test-time training approach that enables diverse, 3D-consistent scene generation.

To summarize, our key contributions are the following:

- (1) The first text-driven perpetual view generation method, which can synthesize long-term videos of diverse domains solely from text and a camera trajectory.
- (2) The first zero-shot/test-time scene generation method, which synthesizes diverse scenes without large-scale training on a specific target domain.

¹Code will be made publicly available.

- (3) Achieving 3D-consistent generation by progressively estimating a unified 3D representation of the scene.

We thoroughly evaluate and ablate our method, demonstrating a significant improvement in quality and 3D consistency over existing methods.

2 RELATED WORK

3D-Consistent View Synthesis from a Single Image. Related to our task, various methods have considered the task of realistic novel view synthesis from a single input image. A surge of methods have proposed to utilize a NeRF [26] as a unified 3D representation [15, 51, 53]. In contrast to the classical use of NeRF, which requires multiple input images from different viewpoints, these methods are trained on a large dataset from a specific domain to learn a generic scene prior. Other 3D representations have been used by various methods, including multi-plane images [48, 56], point clouds which hold high-dimensional features extracted from a single image [37, 49], or textured-mesh representation [12].

In [15], the task is further regularized using the semantic prior learned by CLIP[31], encouraging high similarity between the input image and each novel view in CLIP image embedding space. All these methods require training a model on specific domains and cannot produce perpetual exploration of diverse scenes.

3D-Aware Image Generation. Several generative models have been proposed for enabling 3D-aware image generation, synthesizing an image while interpolating the camera pose. This is done by incorporating a 3D representation explicitly into a generator, e.g., combining a GAN with a NeRF representation [6, 7, 10, 27, 44], or neural surface renderer [29].

These methods have shown impressive results on structured domains such as cars or faces, yet they are difficult to deploy for large, diverse scenes. In [8], this challenge has been tackled by conditioning the radiance field on a 2D grid of floorplan latent codes. Yet, since this is an unconditional GAN, to synthesize novel views from a *given* image, they require to first invert the image into an input latent noise – a challenging task by itself [36]. Recently, [4] proposed to tackle the difficult task of a “generic NeRF” – a single model that can represent a large dataset of scenes, where their key idea is to work with disentangled scene/camera latent representation. Given this model, they then train diffusion models, unconditioned or conditioned on text/image, to generate the latent space distribution. Thus, they can synthesize scene and camera trajectories using input texts or images. However, this method requires heavy supervision, including large-scale training data that contains accurate camera trajectories, which can be obtained reliably mainly for synthetic data. In the case of text-conditioning, they require text-image paired data for training. All mentioned generative models also require extensive training and can represent only specific domains. In contrast, we aim for a much more diverse, flexible, and lightweight generation of arbitrary scenes.

Perpetual View Generation. The task of freely exploring an “infinite scene” dates back to the seminal work [16], which proposed “Infinite Images” – a technique that retrieves images from a large dataset, then transforms and blends them to create a 2D landscape that follows a desired camera path. Recently, this task has been

modernized by various works. Different methods have proposed to synthesize scenes given a single image and camera motion as input (e.g., [13, 19, 21, 22, 35, 38, 49]). For example, synthesizing indoor scenes with controllable camera motion [19, 35, 38, 49], or synthesizing long-range landscapes flythroughs from a single input image and camera trajectory [21, 22]. These methods have demonstrated impressive improvement in the results and creative use of data and self-supervisory signals (e.g., [21, 35]). Concurrently, DiffDreamer proposed to replace the GAN with a conditional diffusion model [5]. However, all existing methods require extensive training on a large-scale dataset to learn a proper generative and geometric prior of a specific target scene domain.

Text-to-video Generation and Editing. Our work follows a broad line of works in the field of text-to-video synthesis. Text2LIVE [3] combines their text-based image editing capabilities with neural atlases [17] to consistently edit a video. Tune-A-Video [50] fine-tunes the attention projections in a diffusion model to attach text and video pairs, to later on, at inference time, edit the video by editing the text prompt. Magic Video [55] uses a diffusion process conditioned on CLIP [31] text encoding in the latent space of a VAE decoder to extract keyframes that are being interpolated and super-resolved into a video. Make-A-Video [45] uses a pre-trained text-image model as a prior to generate frames that are later spatiotemporally resolved to a video.

Text-to-3D Generation and Editing. Recently, image-text pretrained models [31, 41], and differentiable renderers [23, 26], have been utilized for editing or synthesizing 3D content from text. [25] edits the style of a given surface mesh according to an input text, by matching the CLIP features of the rendered images with the CLIP features of the input text. Similarly, [14] uses CLIP loss for synthesizing a NeRF from a single input text. Finally, [30] improved over [14] by constraining the generated NeRF to render images that are in the distribution of a pre-trained text-to-image diffusion model [41], given the input text.

3 METHOD

The input to our method is a text prompt P , describing the target scene, and a camera trajectory denoted by: $\{C_i\}_{i=1}^T$, where C_i is the camera pose for the i^{th} frame. Our goal is to synthesize a long-term, high-quality video that depicts the desired scene while following the camera trajectory.

Our framework, illustrated in Fig. 2, generates the scene in an online fashion, one frame at a time, by leveraging a pre-trained text-to-image diffusion model [39], and a pre-trained monocular depth prediction model [32, 33]. The role of the diffusion model is to synthesize new content that is revealed as the camera moves, whereas the depth prediction model allows us to estimate the geometry of the new generated content. We combine these two models through a unified 3D representation of the scene, which ensures geometrically consistent video generation. More specifically, at each time step t , the new synthesized content and its predicted depths are used to update a unified mesh representation of the scene \mathcal{M} , which is constructed progressively as the camera moves in the scene. The mesh is then projected to the next view C_{t+1} , and the process is repeated.

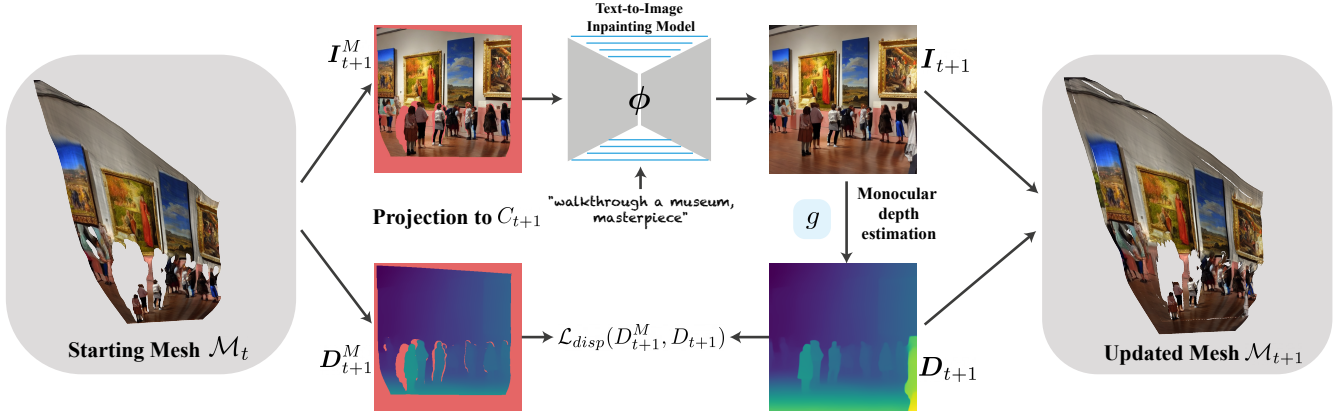


Figure 2: SceneScape pipeline. We represent the generated scene with a unified mesh \mathcal{M} , which is constructed in an online fashion. Given a camera at C_{t+1} , at each synthesis step, a new frame is generated by projecting \mathcal{M}_t into C_{t+1} , and synthesizing the newly revealed content by using a pre-trained text-to-image diffusion model. To estimate the geometry of the new synthesized content, we leverage a pre-trained depth prediction model; to ensure the predicted depth is consistent with the existing scene \mathcal{M}_t , we deploy a test-time training, encouraging the predicted depth by the model to match the projected depth from \mathcal{M}_t . We then update our mesh representation to form \mathcal{M}_{t+1} which includes the new scene content.

Since neither the depth prediction model, nor the inpainting model are guaranteed to produce consistent predictions across time, we finetune them both, at test-time, to match the content of our unified scene representation for the known, previously synthesized content. We next describe each of these components in detail.

3.1 Initialization and Scene Representation

We denote the pre-trained text-to-image inpainting model by ϕ , which takes as input a text prompt P , a mask M , and a masked conditioning image I_t^M :

$$I_t = \phi(M, I_t^M, P) \quad (1)$$

The first frame in our video I_0 is generated by sampling an image from ϕ , using P without masking (all-ones mask). The generated frame is then fed to a pre-trained depth prediction model g , which estimates D_0 the depth map for I_0 , i.e., $D_0 = g(I_0)$.

With the estimated depth and camera poses, a possible approach for rendering I_{t+1} is to warp I_t to C_{t+1} , e.g., using 2D splatting [28]. However, even with consistent depths, rendering a 3D-consistent scene is challenging. In typical camera motion, multiple pixels from one frame are mapped into the same pixel in the next frame. Thus, the aggregated color needs to be selected carefully. Furthermore, frame-to-frame warping lacks a unified representation, thus, once the scene content gets occluded, it will be inpainted from scratch when it gets exposed again.

To address these challenges, we take a different approach and represent the scene with a unified triangle mesh $\mathcal{M} = (V, F, E)$ which is represented by a tuple of vertices (3D location and color), faces and edges, respectively. We initialize \mathcal{M}_0 by unprojecting (I_0, D_0) .

After the first frame is generated, each synthesis step consists of the following main stages:

3.2 Project and Inpaint

The current scene content, represented by the unified mesh representation \mathcal{M}_t , is projected to the next camera C_{t+1} :

$$(I_{t+1}^M, D_{t+1}^M, M) = Proj(\mathcal{M}_t, C_{t+1}) \quad (2)$$

producing a mask M of the visible content in C_{t+1} , a masked frame I_{t+1}^M , and a masked depth map D_{t+1}^M .

Given the projected (masked) frame, we now turn to the task of synthesizing new content. To do so, we apply ϕ using Eq. 1. Since often the new content extends large regions in the image, there is no unique solution to this inpainting task. We thus use ϕ to sample multiple possible continuations of the video $\{I_{t+1}^i\}$, and select the one that most closely aligns with the target text prompt P :

$$\arg \max_i \cos(E_{\text{txt}}(P), E_{\text{img}}(I_{t+1}^i)) \quad (3)$$

where \cos denotes the cosine similarity metric, and $E_{\text{txt}}, E_{\text{img}}$ are the text and image encoder of CLIP [31].

3.3 Test-time Depth Finetuning

We would like to estimate the geometry of the new synthesized content and use it to update our unified scene mesh. A naïve approach to do so is to estimate the depth directly from the inpainted frame, i.e., $D_{t+1} = g(I_{t+1})$. However, monocular depth predictions tend to be inconsistent, even across nearby video frames. That is, there is no guarantee the predicted depth D_{t+1} would be well aligned with the current scene geometry \mathcal{M}_t . We mitigate this problem by taking a test-time training approach to finetune the depth prediction model to be as consistent as possible with the current scene geometry. This approach is inspired by previous methods [20, 24, 54], which encourage pairwise consistency w.r.t optical flow observations in a given video. In contrast, we encourage consistency w.r.t. a unified 3D representation. Formally, our training loss is given by:

$$\mathcal{L}_{disp} = \left\| D_{t+1}^M - g(I_{t+1}) \odot M \right\|_1 \quad (4)$$

To preserve the original prior learned by the depth model, for each generated frame we start by reverting the weights of g to the original depth estimation network weights.

3.4 Test-time Decoder Finetuning

Our framework uses Latent Diffusion inpainting model, in which the input image and mask are first encoded into a latent space $z = E_{\text{LDM}}(M, I_t^M)$; the inpainting operation is then carried out in the latent space, producing \hat{z} , and the final output image is given by decoding \hat{z} to an RGB image: $D_{\text{LDM}}(\hat{z})$. This encoding/decoding operation is lossy, and the encoded image is not reconstructed exactly in the unmasked regions. Following [2], for each frame, we finetune the decoder as follows:

$$\mathcal{L}_{dec} = \left\| D_{\text{LDM}}(\hat{z}) \odot M - I_{t+1}^M \right\|_2 + \left\| (D_{\text{LDM}}(\hat{z}) - D_{\text{LDM}}^{\text{fixed}}(\hat{z})) \odot (1 - M) \right\|_2 \quad (5)$$

where the first term encourages the decoder to preserve the known content, and the second term is a prior preservation loss suggested in [2]. As in Sec. 3.3, we revert the weights of the decoder to its original weights.

3.5 Online Mesh Update

Given the current mesh M_t , and the inpainted frame I_{t+1} , we use our depth map and camera pose to update the scene with the new synthesized content. Note that in order to retain the previously synthesized content, some of which may be occluded in the current view, we consider only the new content, unproject and mesh it, adding it to M_t . That is,

$$\tilde{M}_{t+1} = \text{UnProj}(M, I_{t+1}, D_{t+1}, C_{t+1}) \quad (6)$$

Finally, \tilde{M}_{t+1} is merged into the mesh: $M_{t+1} = M_t \cup \tilde{M}_{t+1} = (V_t \cup \tilde{V}_{t+1}, F_t \cup \tilde{F}_{t+1}, E_t \cup \tilde{E}_{t+1})$

4 RESULTS

We evaluate our method both quantitatively and qualitatively on various scenes generated from a diverse set of prompts, including photorealistic as well as imaginary scenes. We generated 50 frames long videos, with a fast-moving camera motion, which follows a backward motion combined with the panning of the camera. See Appendix (Sec. A) for more details. Since our method represents the scene via a mesh, we focus mainly on indoor scenes. Synthesizing outdoor scenes would require careful handling in cases of dramatic depth discontinuities (see discussion Sec. 5).

Figure 3 shows sample frames from our generated videos. Additional examples as well as our videos and predicted depth maps are included in the Supplementary Materials (SM). As seen, the results demonstrate the effectiveness of our method in producing high-quality and geometrically-plausible scenes, depicting scenes with significant parallax, complex structures, and various complex scene properties such as lighting (e.g., fluorescent lighting, or fire) or diverse materials (e.g., ice).

As for the comparison to prior work, to the best of our knowledge, there is no existing method applicable in our setting – text-driven perpetual view generation of diverse scenes. The most relevant methods (e.g., [21, 35]) require an input image and are trained and evaluated on specific domains. Our framework is not bounded to a specific domain, thus existing evaluation protocols such as FID w.r.t. training data are less meaningful in our case. We thus propose several alternative metrics and provide an extensive ablation of our key components.

4.1 Ablation

We numerically ablate the key components in our framework: (i) depth finetuning, (ii) our decoder finetuning, and (iii) our unified mesh representation. For the first two ablations, we apply our framework without each component, and for the third, we replace our unified mesh with 2D rendering, i.e., warping the content from the current frame to the next, using a depth-aware splatting [28]. We ran these baselines on five diverse videos and measured the following metrics:

Depth consistency. We evaluate the consistency of the depth maps produced by our method compared to the predicted depth by COLMAP [42, 43]. Specifically, we apply COLMAP on our generated videos, using known camera poses, and compute the Scale-Invariant Root Mean Square Error (SI-RMSE) [9]:

$$SI\text{-}RMSE = \sqrt{\frac{1}{N^2} \sum_{p, q \in I} ((\log D^o(p) - D^o(q)) - (\log D^c(p) - D^c(q)))^2} \quad (7)$$

where D^o and D^c are our and COLMAP predicted depths, respectively. This metric measures the squared, log-space difference in depth between two pixels in our prediction and the same two pixels in COLMAP’s predictions, averaged over all pairs of valid pixels. We compute the SI-RMSE for each frame and report the average per video. In addition, to measure the completeness of the reconstruction, we also report the percentage of video pixels recovered by COLMAP, i.e., passed its geometric consistency test.

Pose accuracy. To further assess the 3D consistency of our generated videos, we run COLMAP, this time providing it only the intrinsic parameters. We then measure the accuracy of the estimated camera trajectory, i.e., the extrinsic parameters. We follow [52] and align the two camera systems by computing a global rotation matrix. We then measure the normalized mean accuracy of camera positions (in percentage, relative to the overall camera trajectory), and camera rotations (in degrees).

Table 1 and Table 2 report the above metrics for our method and the baselines. Our full method results in more accurate camera poses, denser reconstructions, and better aligned depth maps compared the baselines. As seen in Table 1, excluding depth finetuning results in inconsistent depth predictions (high *SI-RMSE*), and significantly sparser reconstructions (lower *Density*). In terms of pose accuracy, we observed that COLMAP managed to estimate the pose of early cameras fairly well, even w/o depth finetuning, since we still use a unified 3D representation. However, it fails for distant cameras, which do not share common content with the first image

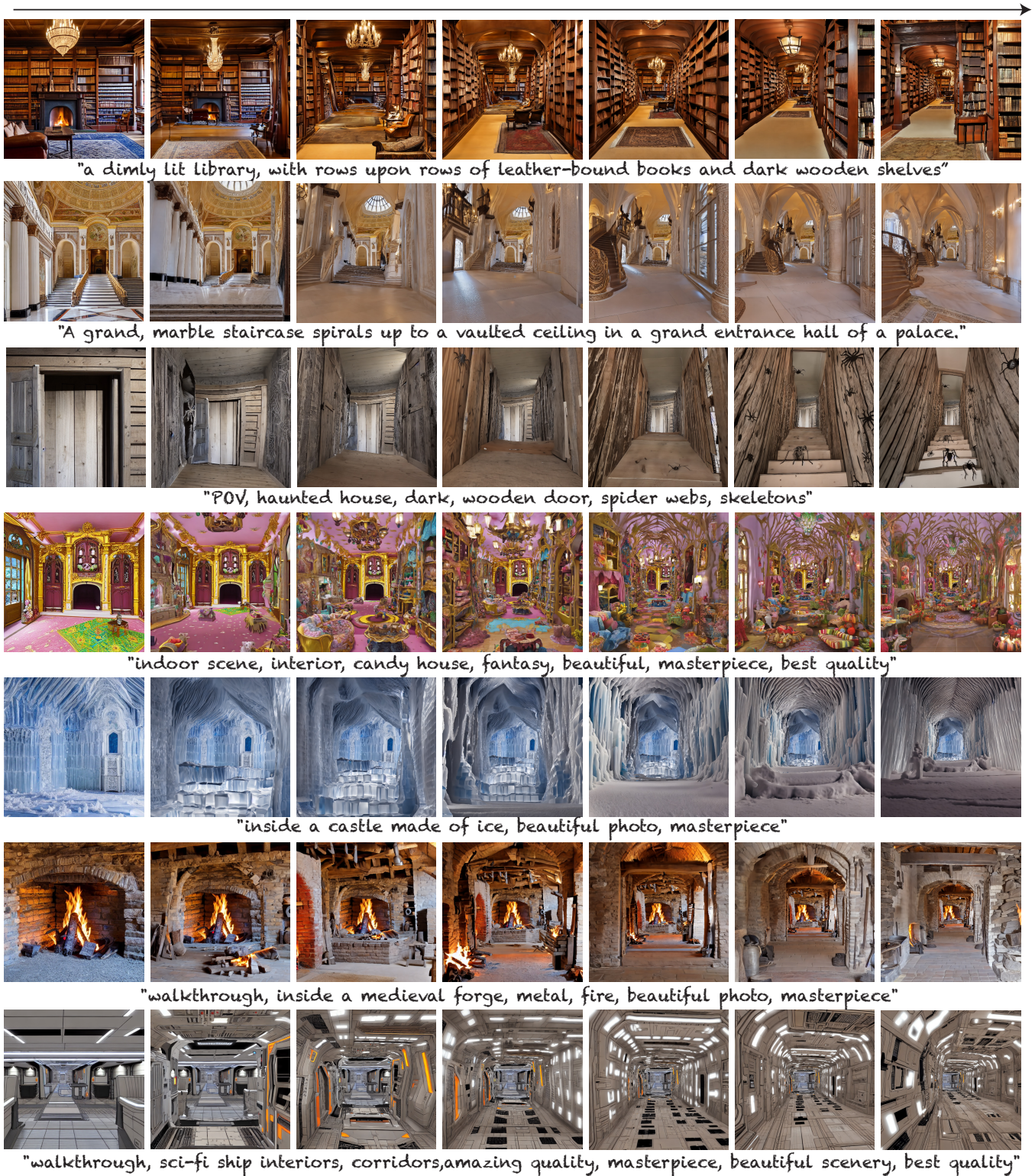


Figure 3: Sample frames from our generated videos. The input text prompt is shown below each example. Our method generates high-quality and diverse scenes, while following a desired camera trajectory.

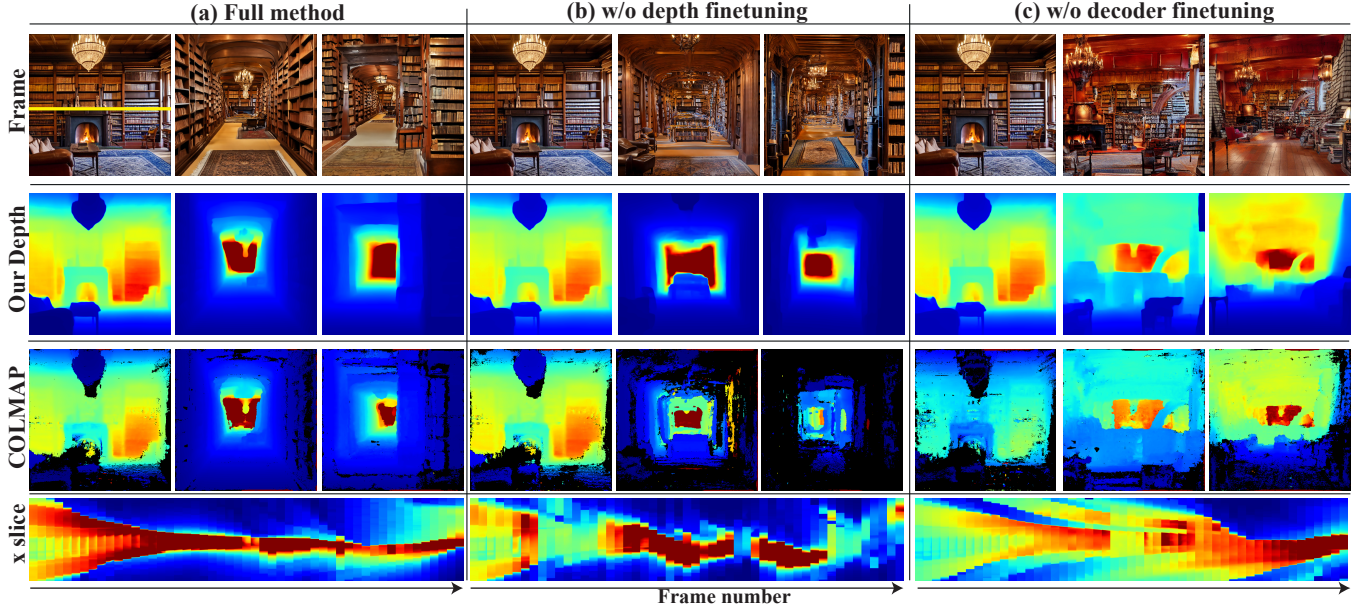


Figure 4: Ablations of our key components: depth finetuning (Sec. 3.3), and decoder finetuning (Sec. 3.4). In each case, we run COLMAP on the generated video and present the estimated depth maps to ours. We also present x-t slices computed on our depth maps (bottom). As seen, both components are essential for obtaining 3D-consistent generation.

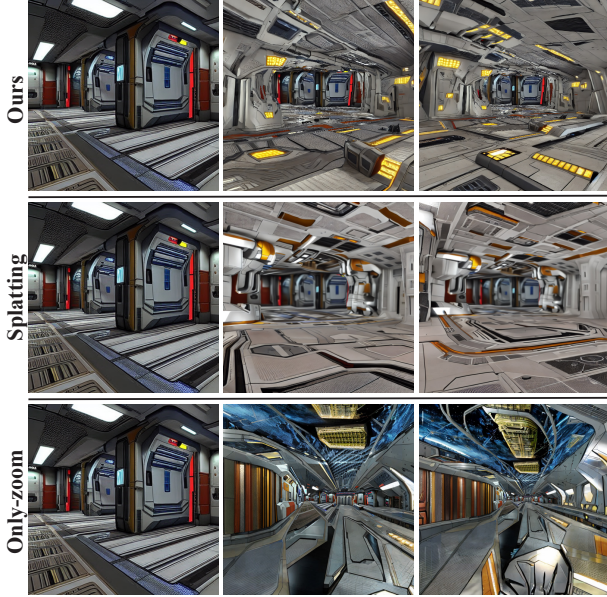


Figure 5: Comparison with: (i) Only-zoom baseline, and (ii) 2D splatting instead of our unified mesh.

(Cameras in Table 2). When depth finetuning is enabled, the geometric consistency and pose accuracy improve, yet the reconstructions are still sparser and less accurate than using our full setting.

Figure 4 shows these results for one of our videos. It also shows that without finetuning the decoder, our generated frames suffer

	SI-RMSE ↓	Density (%) ↑
<i>Ours</i>	0.13 ± 0.02	84.6 ± 4.4
<i>w/o Depth Finetuning</i>	0.65 ± 0.24	54.5 ± 21.5
<i>w/o Decoder Finetuning</i>	0.14 ± 0.03	75.9 ± 3.6
<i>w/o Mesh Representation</i>	0.13 ± 0.04	75 ± 2.27

Table 1: Depth Consistency. We report the Scale Invariant RMSE (SI-RMSE) between the depth produced by each of our ablation baselines, and COLMAP’s dense reconstruction. We also report the average percentage of pixels recovered by COLMAP. See Sec. 4.1 for more details.

	Rotation (degree) ↓	Translation (%) ↓	Cameras (%) ↑
<i>Ours</i>	0.05 ± 0.01	$8 \cdot 10^{-4} \pm 2 \cdot 10^{-4}$	100
<i>w/o Depth F.</i>	0.59 ± 1.03	$3 \cdot 10^{-3} \pm 4 \cdot 10^{-3}$	65 ± 27
<i>w/o Decoder F.</i>	0.08 ± 0.024	$1 \cdot 10^{-3} \pm 3 \cdot 10^{-4}$	100
<i>w/o Mesh R.</i>	0.2 ± 0.03	$1 \cdot 10^{-2} \pm 7 \cdot 10^{-3}$	100

Table 2: Pose Accuracy. For each baseline, we apply COLMAP’s sparse reconstruction, and report the accuracy of the recovered camera poses w.r.t. ground truth ones, and the fraction of reconstructed cameras.

from inconsistent high-frequency content, which affects the depth prediction, and results in a higher COLMAP reconstruction error.

In Fig. 5, we show a qualitative comparison to the 2D splatting baseline. As expected, this method results in blurry content due to repetitive interpolation. Finally, we also include an example of an *only-zoom* baseline, which does not model the scene geometry but rather iteratively scales the image and inpaints it [11]. This comparison demonstrates that modeling the scene with a constant depth is insufficient for synthesizing complex scenes. See SM for videos.

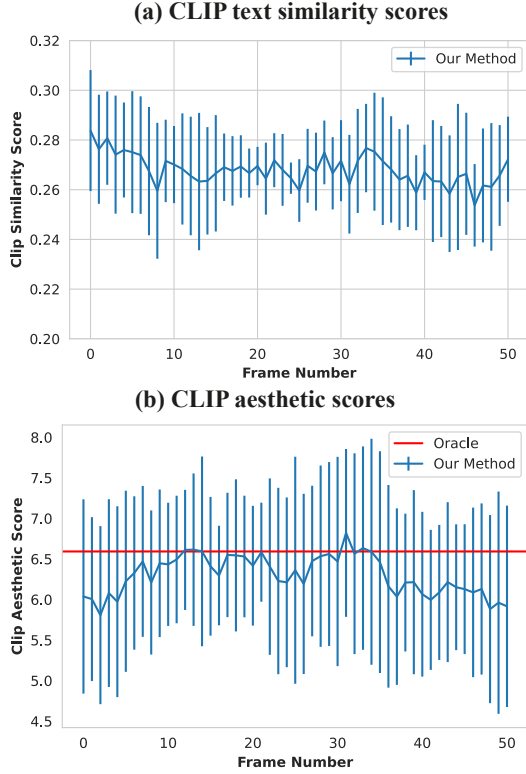


Figure 6: (a) CLIP aesthetic scores of our method compared to “oracle” scores. (b) CLIP text similarity scores. Average across videos used in ablation (mean \pm std)

4.2 Scene Semantics and Visual Quality

To measure how well our generated videos adhere to the desired scene, and to assess the visual quality of our results across time, we use two CLIP-based scores: (i) cosine similarity between each of the generated frames and the input text, and (ii) quality/aesthetic score [1] – an image aesthetic linear predictor learned on top of CLIP embeddings.

As shown in Fig. 6(a), our method preserves the same fidelity to the input text prompt throughout the entire video generation. In addition, Fig. 6(b) shows that the visual quality of our generated frames is largely preserved across time. For reference, we also include an “oracle” score (in red), computed over 50 sampled images using the same prompts in our video generation.

5 DISCUSSION AND CONCLUSION

We posed the task of text-driven perpetual scene generation and proposed a test-time training approach to generate long-term videos of diverse scenes. Our framework demonstrates two key principles: (i) how to harness two powerful pre-trained models for this task, allowing us to generate scenes in a zero-shot manner without requiring any training data from a specific domain, and (ii) how to combine these models with a unified 3D representation of the scene, which by construction ensures geometry consistency of the generated video, and enables high quality and efficient rendering.



Figure 7: Limitation. Outdoor scenes are poorly represented with our mesh representation (top). In addition, for longer-term videos, we may observe degradation in quality, due to error accumulation (bottom).

As for limitations, the quality of our results depends on the generative and geometric priors and may sometime decrease over time (Fig. 7 bottom), and may result in a distorted geometry or artifacts for longer-term videos. In addition, as mentioned in Sec. 4, since we represent the scene with triangular mesh, it is difficult for our method to represent dramatic depth discontinuities, e.g., sky vs. ground in outdoor scenes (Fig. 7 top). Devising a new 3D scene representation tailored for the perpetual view generation of arbitrary scenes is an intriguing avenue of future research. We believe that the principles demonstrated in our work hold great promise in developing lightweight, 3D-aware video generation methods.

6 ACKNOWLEDGMENTS

We thank Shai Bagon for his insightful comments. We thank Narek Tumanyan for his help with the website creation. This project received funding from the Israeli Science Foundation (grant 2303/20).

REFERENCES

- [1] LAION AI. 2022. CLIP Aesthetic Score Predictor. <https://github.com/LAION-AI/aesthetic-predictor>. Accessed: 2023-01-25.
- [2] Omri Avrahami, Ohad Fried, and Dani Lischinski. 2022. Blended Latent Diffusion. *CoRR* abs/2206.02779 (2022). <https://doi.org/10.48550/arXiv.2206.02779>
- [3] Omer Bar-Tal, Dolev Ofri-Amar, Rafail Fridman, Yoni Kasten, and Tali Dekel. 2022. Text2live: Text-driven layered image and video editing. In *ECCV*.
- [4] Miguel Angel Bautista, Pengsheng Guo, Samira Abnar, Walter Talbott, Alexander Toshev, Zhuoyuan Chen, Laurent Dinh, Shuangfei Zhai, Hanlin Goh, Daniel Ulbricht, et al. 2022. Gaudi: A neural architect for immersive 3d scene generation. *arXiv preprint arXiv:2207.13751* (2022).
- [5] Sheng Cai, Eric Chan, Songyou Peng, Mohamad Shahbazi, Anton Obukhov, Luc Van Gool, and Gordon Wetzstein. 2022. DiffDreamer: Consistent Single-view Perpetual View Generation with Conditional Diffusion Models. *ArXiv* abs/2211.12131 (2022).
- [6] Eric Chan, Marco Monteiro, Petr Kellnhofer, Jiajun Wu, and Gordon Wetzstein. 2021. pi-GAN: Periodic Implicit Generative Adversarial Networks for 3D-Aware Image Synthesis. In *Proc. CVPR*.
- [7] Eric R. Chan, Connor Z. Lin, Matthew A. Chan, Koki Nagano, Boxiao Pan, Shalini De Mello, Orazio Gallo, Leonidas Guibas, Jonathan Tremblay, Sameh Khamis, Tero Karras, and Gordon Wetzstein. 2022. Efficient Geometry-aware 3D Generative Adversarial Networks. In *CVPR*.
- [8] Terrance DeVries, Miguel Angel Bautista, Nitish Srivastava, Graham W Taylor, and Joshua M Susskind. 2021. Unconstrained scene generation with locally conditioned radiance fields. In *Proceedings of the IEEE/CVF International Conference on Computer Vision*. 14304–14313.
- [9] David Eigen, Christian Puhrsch, and Rob Fergus. 2014. Depth map prediction from a single image using a multi-scale deep network. *Advances in neural information processing systems* (2014).
- [10] Jiatao Gu, Lingjie Liu, Peng Wang, and Christian Theobalt. 2021. StyleNeRF: A Style-based 3D-Aware Generator for High-resolution Image Synthesis. *ArXiv* abs/2110.08985 (2021).
- [11] David Ha. 2022. Experimenting with infinite zoom out using StableDiffusion2. <https://twitter.com/hardmaru/status/1611569188144807943>. Accessed: 2023-01-25.
- [12] Ronghang Hu, Nikhila Ravi, Alexander C. Berg, and Deepak Pathak. 2021. World-sheet: Wrapping the World in a 3D Sheet for View Synthesis from a Single Image. In *Proceedings of the IEEE International Conference on Computer Vision (ICCV)*.
- [13] Ronghang Hu, Nikhila Ravi, Alexander C. Berg, and Deepak Pathak. 2021. World-sheet: Wrapping the World in a 3D Sheet for View Synthesis from a Single Image. In *ICCV*.
- [14] Ajay Jain, Ben Mildenhall, Jonathan T. Barron, Pieter Abbeel, and Ben Poole. 2022. Zero-Shot Text-Guided Object Generation with Dream Fields. (2022).
- [15] Ajay Jain, Matthew Tancik, and Pieter Abbeel. 2021. Putting NeRF on a Diet: Semantically Consistent Few-Shot View Synthesis. In *Proceedings of the IEEE/CVF International Conference on Computer Vision (ICCV)*. 5885–5894.
- [16] Biliana Kaneva, Josef Sivic, Antonio Torralba, Shai Avidan, and William T. Freeman. 2010. Infinite Images: Creating and Exploring a Large Photorealistic Virtual Space. *Proc. IEEE* (2010).
- [17] Yoni Kasten, Dolev Ofri, Oliver Wang, and Tali Dekel. 2021. Layered neural atlases for consistent video editing. *ACM Transactions on Graphics (TOG)* 40 (2021), 1–12.
- [18] Diederik P. Kingma and Jimmy Ba. 2014. Adam: A Method for Stochastic Optimization. *CoRR* abs/1412.6980 (2014).
- [19] Jing Yu Koh, Honglak Lee, Yinfei Yang, Jason Baldridge, and Peter Anderson. 2021. Pathdreamer: A World Model for Indoor Navigation. *ICCV*.
- [20] Johannes Kopf, Xuejian Rong, and Jia-Bin Huang. 2021. Robust Consistent Video Depth Estimation. In *IEEE/CVF Conference on Computer Vision and Pattern Recognition*.
- [21] Zhengqi Li, Qianqian Wang, Noah Snavely, and Angjoo Kanazawa. 2022. Infinitenature-zero: Learning perpetual view generation of natural scenes from single images. In *Computer Vision–ECCV 2022: 17th European Conference, Tel Aviv, Israel, October 23–27, 2022, Proceedings, Part I*. Springer, 515–534.
- [22] Andrew Liu, Richard Tucker, Varun Jampani, Ameesh Makadia, Noah Snavely, and Angjoo Kanazawa. 2021. Infinite nature: Perpetual view generation of natural scenes from a single image. In *Proceedings of the IEEE/CVF International Conference on Computer Vision*. 14458–14467.
- [23] Shichen Liu, Tianye Li, Weikai Chen, and Hao Li. 2019. Soft Rasterizer: A Differentiable Renderer for Image-based 3D Reasoning. *The IEEE International Conference on Computer Vision (ICCV)* (Oct 2019).
- [24] Xuan Luo, Jia-Bin Huang, Richard Szeliski, Kevin Matzen, and Johannes Kopf. 2020. Consistent Video Depth Estimation. 39, 4 (2020).
- [25] Oscar Michel, Roi Bar-On, Richard Liu, Sagie Benaim, and Rana Hanocka. 2022. Text2Mesh: Text-Driven Neural Stylization for Meshes. In *Proceedings of the IEEE/CVF Conference on Computer Vision and Pattern Recognition (CVPR)*. 13492–13502.
- [26] Ben Mildenhall, Pratul P. Srinivasan, Matthew Tancik, Jonathan T. Barron, Ravi Ramamoorthi, and Ren Ng. 2020. NeRF: Representing Scenes as Neural Radiance Fields for View Synthesis. In *European Conference on Computer Vision*.
- [27] Michael Niemeyer and Andreas Geiger. 2020. GIRAFFE: Representing Scenes as Compositional Generative Neural Feature Fields. *2021 IEEE/CVF Conference on Computer Vision and Pattern Recognition (CVPR)* (2020), 11448–11459.
- [28] Simon Niklaus and Feng Liu. 2020. Softmax splatting for video frame interpolation. In *Proceedings of the IEEE/CVF Conference on Computer Vision and Pattern Recognition*. 5437–5446.
- [29] Roy Or-El, Xuan Luo, Mengyi Shan, Eli Shechtman, Jeong Joon Park, and Ira Kemelmacher-Shlizerman. 2022. StyleSDF: High-Resolution 3D-Consistent Image and Geometry Generation. In *Proceedings of the IEEE/CVF Conference on Computer Vision and Pattern Recognition (CVPR)*. 13503–13513.
- [30] Ben Poole, Ajay Jain, Jonathan T. Barron, and Ben Mildenhall. 2022. DreamFusion: Text-to-3D using 2D Diffusion. *arXiv* (2022).
- [31] Alec Radford, Jong Wook Kim, Chris Hallacy, Aditya Ramesh, Gabriel Goh, Sandhini Agarwal, Girish Sastry, Amanda Askell, Pamela Mishkin, Jack Clark, Gretchen Krueger, and Ilya Sutskever. 2021. Learning Transferable Visual Models From Natural Language Supervision. In *International Conference on Machine Learning*.
- [32] René Ranftl, Alexey Bochkovskiy, and Vladlen Koltun. 2021. Vision Transformers for Dense Prediction. *ICCV* (2021).
- [33] René Ranftl, Katrin Lasinger, David Hafner, Konrad Schindler, and Vladlen Koltun. 2022. Towards Robust Monocular Depth Estimation: Mixing Datasets for Zero-Shot Cross-Dataset Transfer. *IEEE Transactions on Pattern Analysis and Machine Intelligence* 44, 3 (2022).
- [34] Nikhila Ravi, Jeremy Reizenstein, David Novotny, Taylor Gordon, Wan-Yen Lo, Justin Johnson, and Georgia Gkioxari. 2020. Accelerating 3D Deep Learning with PyTorch3D. *arXiv:2007.08501* (2020).
- [35] Xuanchi Ren and Xiaolong Wang. 2022. Look Outside the Room: Synthesizing A Consistent Long-Term 3D Scene Video from A Single Image. In *CVPR*.
- [36] Elad Richardson, Yuval Alaluf, Or Patashnik, Yotam Nitzan, Yaniv Azar, Stav Shapiro, and Daniel Cohen-Or. 2021. Encoding in Style: a StyleGAN Encoder for Image-to-Image Translation. In *IEEE/CVF Conference on Computer Vision and Pattern Recognition (CVPR)*.
- [37] Chris Rockwell, David F. Fouhey, and Justin Johnson. 2021. PixelSynth: Generating a 3D-Consistent Experience from a Single Image. In *ICCV*.
- [38] Chris Rockwell, David F. Fouhey, and Justin Johnson. 2021. PixelSynth: Generating a 3D-Consistent Experience from a Single Image. In *ICCV*.
- [39] Robin Rombach, Andreas Blattmann, Dominik Lorenz, Patrick Esser, and Björn Ommer. 2022. High-Resolution Image Synthesis With Latent Diffusion Models. In *Proceedings of the IEEE/CVF Conference on Computer Vision and Pattern Recognition (CVPR)*. 10684–10695.
- [40] Robin Rombach, Patrick Esser, and Björn Ommer. 2021. Geometry-Free View Synthesis: Transformers and no 3D Priors. *arXiv:2104.07652 [cs.CV]*
- [41] Chitwan Saharia, William Chan, Saurabh Saxena, Lala Li, Jay Whang, Emily L. Denton, Seyed Kamyar Seyed Ghasemipour, Burcu Karagol Ayan, Seyedeh Sara Mahdavi, Raphael Gontijo Lopes, Tim Salimans, Jonathan Ho, David Fleet, and Mohammad Norouzi. 2022. Photorealistic Text-to-Image Diffusion Models with Deep Language Understanding.
- [42] Johannes Lutz Schönberger and Jan-Michael Frahm. 2016. Structure-from-Motion Revisited. In *Conference on Computer Vision and Pattern Recognition (CVPR)*.
- [43] Johannes L. Schönberger, Enliang Zheng, Jan-Michael Frahm, and Marc Pollefeys. 2016. Pixelwise View Selection for Unstructured Multi-View Stereo. In *European Conference on Computer Vision*.
- [44] Katja Schwarz, Yiyi Liao, Michael Niemeyer, and Andreas Geiger. 2020. Graf: Generative radiance fields for 3d-aware image synthesis. *Advances in Neural Information Processing Systems* 33 (2020), 20154–20166.
- [45] Uriel Singer, Adam Polyak, Thomas Hayes, Xiaoyue Yin, Jie An, Songyang Zhang, Qiyuan Hu, Harry Yang, Oron Ashual, Oran Gafni, Devi Parikh, Sonal Gupta, and Yaniv Taigman. 2022. Make-A-Video: Text-to-Video Generation without Text-Video Data. *ArXiv* abs/2209.14792 (2022).
- [46] Jiaming Song, Chenlin Meng, and Stefano Ermon. 2020. Denoising diffusion implicit models. *arXiv preprint arXiv:2010.02502* (2020).
- [47] Alexandru Cristian Telea. 2004. An Image Inpainting Technique Based on the Fast Marching Method. *Journal of Graphics Tools* 9 (2004), 23–34.
- [48] Richard Tucker and Noah Snavely. 2020. Single-view view synthesis with multi-plane images. In *Proceedings of the IEEE/CVF Conference on Computer Vision and Pattern Recognition*. 551–560.
- [49] Olivia Wiles, Georgia Gkioxari, Richard Szeliski, and Justin Johnson. 2020. SynSin: End-to-End View Synthesis From a Single Image. In *CVPR*.
- [50] Jay Zhangjie Wu, Yixiao Ge, Xintao Wang, Weixian Lei, Yuchao Gu, Wynne Hsu, Ying Shan, Xiaohu Qie, and Mike Zheng Shou. 2022. Tune-A-Video: One-Shot Tuning of Image Diffusion Models for Text-to-Video Generation. *ArXiv* abs/2212.11565 (2022).
- [51] DeJia Xu, Yifan Jiang, Peihao Wang, Zhiwen Fan, Humphrey Shi, and Zhangyang Wang. 2022. SinNeRF: Training Neural Radiance Fields on Complex Scenes from a Single Image. *arXiv preprint arXiv:2204.00928*.

- [52] Lior Yariv, Yoni Kasten, Dror Moran, Meirav Galun, Matan Atzmon, Basri Ronen, and Yaron Lipman. 2020. Multiview Neural Surface Reconstruction by Disentangling Geometry and Appearance. *Advances in Neural Information Processing Systems* 33 (2020).
- [53] Alex Yu, Vickie Ye, Matthew Tancik, and Angjoo Kanazawa. 2021. pixelNeRF: Neural Radiance Fields from One or Few Images. In *CVPR*.
- [54] Zhoutong Zhang, Forrester Cole, Richard Tucker, William T Freeman, and Tali Dekel. 2021. Consistent depth of moving objects in video. *ACM Transactions on Graphics (TOG)* 40, 4 (2021), 1–12.
- [55] Daquan Zhou, Weimin Wang, Hanshu Yan, Weiwei Lv, Yizhe Zhu, and Jiashi Feng. 2022. MagicVideo: Efficient Video Generation With Latent Diffusion Models. *ArXiv abs/2211.11018* (2022).
- [56] Tinghui Zhou, Richard Tucker, John Flynn, Graham Fyffe, and Noah Snavely. 2018. Stereo magnification: Learning view synthesis using multiplane images. *arXiv preprint arXiv:1805.09817* (2018).

A IMPLEMENTATION DETAILS

We provide implementation details for our framework and finetuning/generation regime.

A.1 Depth Prediction Model and LDM Decoder Finetuning

We use MiDaS-DPT Large [32] as our depth prediction model. For each generated frame, we finetune it for 300 epochs, using Adam optimizer [18] with a learning rate of $1e-7$. Additionally, we revert the weights of the depth prediction model to the initial state, as discussed in Sec. 3.3. We finetune the LDM decoder for 100 epochs on each generation step using Adam optimizer with a learning rate of $1e-4$.

A.2 Frame Generation Configuration

To perform inpainting, we utilize the Stable Diffusion [39] model that was additionally finetuned on the inpainted task. For each

generated frame, we use DDIM scheduler [46] with 50 sampling steps. We use batch size $b = 3$, from which we pick the result whose CLIP embedding has the best cosine similarity score with the inpainting prompt CLIP text embedding (Sec. 3.1).

We generate videos of 50 frames in length. Our camera follows a rotational motion combined with translation in the negative depth direction. Starting from a simple translation for k frames, every n frames we randomly sample a new rotation direction in the x-z plane (panning), that camera follows for n frames. In our experiments, we set $k = 5$ and $n = 5$. We utilize Pytorch3D [34] to perform rendering and update our unified 3d representation.

We observed that the scene’s geometry sometimes induces out-of-distribution inpainting masks for the Stable Diffusion inpainting model. To address this issue, we perform a morphological open operation on the inpainting mask: $M_O = Open(M)$ with a kernel size 3. Then we inpaint the mask difference $M - M_O$ using [47], while the inpainting model operates on M_O afterward.

A.3 Image to Mesh Unprojection

Given an image I_{t+1} , a mask of pixels to unproject M , a corresponding depth map D_{t+1} and a camera pose C_{t+1} , we unproject the content in a process that is denoted in the main paper by $\tilde{M}_{t+1} = UnProj(M, I_{t+1}, D_{t+1}, C_{t+1})$. First, each pixel center is unprojected by its depth value and camera pose into a 3D mesh vertex with the pixel’s color as its vertex color. Then, each unprojected four neighboring pixels with coordinates (i, j) , $(i + 1, j)$, $(i, j + 1)$, $(i + 1, j + 1)$ are used to define two adjacent triangle faces.